



Published in final edited form as:

Geophys Res Lett. 2017 June 28; 44(12): 6145–6153. doi:10.1002/2017GL073904.

Joint Sentinel-1 and SMAP data assimilation to improve soil moisture estimates

H. Lievens^{1,2}, R. H. Reichle², Q. Liu^{2,3}, G. J. M. De Lannoy⁴, R. S. Dunbar⁵, S. B. Kim⁵, N. N. Das⁵, M. Cosh⁶, J. P. Walker⁷, and W. Wagner⁸

¹Laboratory of Hydrology and Water Management, Ghent University, Ghent, Belgium

²Global Modeling and Assimilation office, NASA Goddard Space Flight Center, Greenbelt, MD, USA

³Science Systems and Applications, Lanham, MD, USA

⁴Department of Earth and Environmental Sciences, KU Leuven, Heverlee, Belgium

⁵Jet Propulsion Laboratory, California Institute of Technology, Pasadena, CA, USA

⁶Hydrology and Remote Sensing Laboratory, USDA-ARS, Beltsville, MD, USA

⁷Department of Civil Engineering, Monash University, Melbourne, Victoria, Australia

⁸Department of Geodesy and Geoinformation, Vienna University of Technology, Vienna, Austria

Abstract

SMAP (Soil Moisture Active and Passive) radiometer observations at ~40 km resolution are routinely assimilated into the NASA Catchment Land Surface Model to generate the 9-km SMAP Level-4 Soil Moisture product. This study demonstrates that adding high-resolution radar observations from Sentinel-1 to the SMAP assimilation can increase the spatio-temporal accuracy of soil moisture estimates. Radar observations were assimilated either separately from or simultaneously with radiometer observations. Assimilation impact was assessed by comparing 3-hourly, 9-km surface and root-zone soil moisture simulations with *in situ* measurements from 9-km SMAP core validation sites and sparse networks, from May 2015 to December 2016. The Sentinel-1 assimilation consistently improved surface soil moisture, whereas root-zone impacts were mostly neutral. Relatively larger improvements were obtained from SMAP assimilation. The joint assimilation of SMAP and Sentinel-1 observations performed best, demonstrating the complementary value of radar and radiometer observations.

1 Introduction

The global water, energy and carbon cycles are linked through the moisture contained in the soil surface and root-zone. Surface soil moisture controls the partitioning of precipitation into runoff and infiltration, energy is dissipated through the evaporation and transpiration of surface and root-zone moisture, and transpiration is linked to CO₂ uptake by plants. As the

crucial link between these cycles, soil moisture is considered an essential climate variable [World Meteorological Organization, 2006].

Past decades have drawn an increasing interest towards constraining soil moisture simulations from land surface models (LSM) through the assimilation of different kinds of satellite microwave observations. Radiometer and scatterometer missions provide coarse (25–40 km) but frequent (~daily) observations, while synthetic aperture radar (SAR) missions achieve high resolution (1m to 1 km) but with infrequent revisit times (several days to weeks).

With the increasing availability of new types of satellite observations emerges the opportunity to explore their synergistic use [Su et al., 2014]. This study follows Draper et al. [2012], who assimilated soil moisture retrievals from active and passive microwave observations and found that for maximum accuracy and coverage both should be assimilated together. Here, we investigated the joint assimilation of SMAP (Soil Moisture Active and Passive, Entekhabi et al. [2010]) and Sentinel-1 [Geudtner, 2012] observations for improving estimates of soil moisture. The SMAP L-band radiometer provides ~daily brightness temperature (TB) observations at ~40-km resolution, which are routinely assimilated into the GEOS-5 (Goddard Earth Observing System version 5) CLSM (Catchment Land Surface Model, Koster et al. [2000]) to generate the 9-km SMAP Level-4 Soil Moisture product [Reichle et al., 2017]. Sentinel-1, a constellation of two (A and B) satellites with C-band SAR, provides backscatter (σ^0) observations at $5 \times 20\text{m}^2$ resolution. The integration of Sentinel-1 σ^0 observations into the assimilation system designed for SMAP is appealing in several ways:

1. Sentinel-1 is the first SAR constellation with 6-day repeat cycle, offering sufficiently frequent revisits for data assimilation. Revisit times of previous SAR missions permit only infrequent assimilation updates that could not be expected to increase the skill of the model estimates significantly.
2. Sentinel-1 C-band σ^0 and SMAP L-band TB observations are complementary. SMAP observations show a higher sensitivity to soil moisture, allowing for more accurate estimation over large spatial scales, whereas Sentinel-1 observations offer increased spatial detail which can potentially bridge the scale-gap between radiometer observations and LSMs operating at increasingly finer resolutions [Wood et al., 2011; Su et al., 2014].
3. The joint assimilation offers an alternative to the off-line downscaling of SMAP TB observations with Sentinel-1 σ^0 , and is not restricted to synchronized overpasses, i.e., it can be performed if either Sentinel-1 or SMAP observations (or both) are available.
4. The direct assimilation of σ^0 observations, instead of the corresponding soil moisture retrievals, circumvents the need for (operational) soil moisture products. While such products are in development for Sentinel-1, the σ^0 assimilation can readily be extended to other SAR missions, such as the RADARSAT constellation, for which soil moisture products are currently lacking.

Finally, the impact of Sentinel-1 σ^o assimilation is a useful measure of the mission's value for estimating surface and root-zone soil moisture, which are key to a better understanding of the water cycle.

2 Data and methods

2.1 Remote sensing observations

SMAP Level-1C TB observations [Chan et al., 2016] in vertical (V) and horizontal (H) polarization on the 36-km EASE-2 (Equal Scalable Earth version 2.0) grid were assimilated from May 2015 to December 2016. The study domain covers parts of the eastern USA, western Europe, the Sahel, and southeastern Australia (Figure 1 a–d, respectively). The observations were masked out over grid cells that included more than 5% open water or glaciated surfaces (based on the GEOS-5 land mask, Mahanama et al. [2015]), or were contaminated by radio frequency interference (RFI).

Sentinel-1A (Sentinel-1B) backscatter data were assimilated starting May 2015 (October 2016) until December 2016. The Level-1 observations in VV-polarization were preprocessed from their native $5 \times 20\text{m}^2$ resolution to the 1-km EASE-2 grid. Sentinel-1 data were excluded for grid cells with more than 1% coverage by open water, urban area, flooded area, permanent ice or snow, and more than 60% coverage by forests, based on 1-km land cover data [Tuanmu and Jetz, 2014]. Areas with complex topography were masked out using a 2.5° threshold for surface slope, derived from 90-m Shuttle Radar Topography Mission elevation data. The thinned dataset was subsequently aggregated linearly to the 9-km EASE-2 grid, provided that 60% of the 1-km grid cells within a given 9-km grid cell contained valid data. Finally, observations were normalized to a reference incidence angle. While Sentinel-1 cycles repeatedly in the same orbital plane, targets on Earth are illuminated at only a limited set of angles, reducing the potential of regression techniques, as applied for normalizing ASCAT data [Bartalis et al., 2006]. Therefore, incidence angle normalization was performed by rescaling the mean σ^o over successive 0.3° angle bins to the mean of the angle bin having the most observations. An advantage of this method is that it simultaneously corrects azimuthal biases [Bartalis et al., 2006]. A limitation is the reduction in accuracy for angle bins with a low number of observations. Therefore, bins with fewer than 15 observations were withdrawn; as more observations become available, the errors in the incidence-angle normalization decrease.

In a final quality control step, SMAP and Sentinel-1 observations were masked out for times and locations where the snow water equivalent (SWE) exceeded 10^{-4} kg/m^2 , the modeled surface temperature (tp1) was less than 273.25 K, or the precipitation (Pcp) exceeded 50 mm/d, based on CLSM estimates from the assimilation system. On average, the time interval between assimilated observations was about 10 times shorter for SMAP than for Sentinel-1 (Figure 1). For SMAP, the interval was generally around 1 day, except for areas in Europe that were affected by RFI in SMOS observations needed for bias correction (Section 2.4). For Sentinel-1, a 6-day interval was achieved over Europe (based primarily on just Sentinel-1A). Other continents were less frequently observed (once every 10–20 days). Recent modifications to the observing schedule increase the Sentinel-1 data availability over the (nearly) global land surface to match that over Europe.

2.2 *In situ* measurements

In situ surface (sfmc) and root-zone (rzmc) soil moisture measurements were assembled over SMAP core validation sites [Colliander et al., 2017] and sparse networks. At core sites, accurate measurements are available at the 9-km scale of the assimilation estimates for a limited set of conditions. Sparse networks cover a wider range of conditions, but are point estimates within a larger model grid cell, and thus subject to scaling errors. The specific validation sites used here are listed in Table 1, with locations shown in Figure 1.

The sfmc measurements correspond to a depth of 5 cm. For core sites, rzmc measurements were vertically averaged with weights proportional to sensor depths within the 0–100 cm layer [Reichle et al., 2016]. For sparse networks, measurements were extracted at single depths, i.e., 20 cm for SCAN, USCRN and SMOSMANIA, 25 cm for Oklahoma Mesonet, and 45 cm for OzNet [De Lannoy and Reichle, 2016a; Reichle et al., 2016].

A strict quality control was performed to remove artifacts, such as spikes, inhomogeneities, oscillations, or trends following Liu et al. [2011]; Entekhabi et al. [2014]; De Lannoy et al. [2014a]. Similar to the remote sensing observations, *in situ* measurements were masked out if CLSM SWE > 10⁻⁴ kg/m², tp1 < 273.25 K, or Pcp > 50 mm/d. Only sites with more than 1000 (3-hourly) measurements within the validation period (May 2015 to December 2016) were included.

2.3 Models

CLSM was run on the 9-km EASE-2 grid using hourly 0.25° × 0.3125° meteorological forcings from the GEOS-5 Forward Processing system [Lucchesi, 2013] with precipitation corrections similar to those of the Level-4 Soil Moisture system [Reichle and Liu, 2014; Reichle et al., 2017]. The CLSM sfmc (0–5 cm) and rzmc (0–100 cm) were diagnosed from three model prognostic variables, the catchment deficit (catdef), surface excess (srfexc) and root-zone excess (rzexc), which represent the equilibrium profile and deviations from equilibrium in the surface and root-zone layers, respectively.

TB simulations were obtained using the zero-order $\tau - \omega$ radiative transfer model (RTM), with input-use of CLSM sfmc, surface soil temperature, air temperature, and climatological leaf area index (LAI) from the Moderate Resolution Imaging Spectroradiometer (MOD15A2). The RTM was calibrated over each 9-km grid cell to minimize biases in the mean and variance between TB simulations and observations [De Lannoy et al., 2013, 2014b]. The calibration was performed over a 4-year period from July 2010 to June 2014 using TB observations from the SMOS (Soil Moisture and Ocean Salinity) mission [Kerr et al., 2001].

Backscatter was simulated by the Water Cloud Model (WCM, Attema and Ulaby [1978]) as the sum of vegetation σ° and attenuated soil σ° . The vegetation σ° and attenuation were modeled as a function of LAI, and soil σ° was a linear function of the CLSM sfmc. Note that a linear soil model was preferred over physically-based models (e.g., the Integral Equation Model, Fung [1994]), which often saturate at moist conditions [Wagner et al., 2010] and cause unrealistically suppressed variability in σ° , particularly if the LSM is (regionally) exposed to wet biases [Lievens et al., 2016]. Due to the limited availability of

Sentinel-1 data, the WCM was calibrated per 9-km grid cell [Lievens et al., 2016] over the same period as used for the validation. Future research should address the validation using independent data.

2.4 Data assimilation

The three-dimensional (3D) Ensemble Kalman Filter (EnKF) [De Lannoy and Reichle, 2016b] was used to assimilate multiple SMAP observations located within a circular (1.25° radius) area around a given 9-km model grid cell. The 3D filter takes into account that SMAP observations have a footprint that is larger than the model resolution. The native Sentinel-1 observations have a footprint that is much smaller than the model resolution. Therefore, the aggregated (9-km) Sentinel-1 observations were used to constrain only the matching 9-km grid cells (1D filter). If both SMAP and Sentinel-1 observations were available simultaneously, the analysis in the joint assimilation proceeded sequentially: First, a 3D analysis was conducted using the SMAP observations. Thereafter, Sentinel-1 observations were used in a 1D analysis to update the estimates from the 3D SMAP analysis.

The model state vector contained $\text{sr}f\text{exc}$, rzexc and catdef (Section 2.3). The forecast error variance was calculated from 24 ensemble trajectories, obtained by perturbing forcings (precipitation, shortwave and longwave radiation) and state variables (catdef and $\text{sr}f\text{exc}$) [De Lannoy and Reichle, 2016a]. The observation error variance for SMAP TB was set to 4^2 K^2 [Reichle et al., 2017], with an isotropic spatial error correlation length of 0.25° . The Sentinel-1 σ° observation error variance was set to 0.3^2 dB^2 [Lievens et al., 2016]. Since Sentinel-1 observations were greatly over-sampled, observation errors were assumed uncorrelated over space. Finally, TB and σ° observation errors were assumed uncorrelated.

The model forecasts can be biased against the observations despite the calibration of the $\tau - \omega$ model and the WCM. To reduce the impact of biases, the assimilation used observation anomalies from the seasonal cycle that were added to the forecast seasonal cycle. The SMAP TB seasonal cycle was calculated from ~ 4 years of SMOS data [De Lannoy and Reichle, 2016a]. This method does not address errors that arise from using climatological vegetation parameters when the (true) vegetation varies from year to year. Given the short (~ 1.5 years) data record, Sentinel-1 σ° anomalies were calculated by subtracting a 6-month moving average from the times series, which reduced errors from vegetation, but may have also partly removed soil moisture information. A relatively long (6-month) window was selected to minimize this artifact, and to increase the number of observations for characterizing the seasonal cycle.

2.5 Experiments

The following experiments were performed:

1. OL: Open loop reference, mean of a 24-member, model-only ensemble simulation without any data assimilation.
2. DA_{σ° : Assimilation of Sentinel-1 σ° (1D-EnKF).
3. DA_{TB} : Assimilation of SMAP TB (3D-EnKF).

4. $DA_{\sigma;TB}$: Joint assimilation of Sentinel-1 and SMAP observations in 1D and 3D analysis configuration, respectively.

The assimilation experiments feature different increment characteristics (Figure 2). Besides the narrower swath, increments of DA_{σ} were spatially more refined than corresponding increments of DA_{TB} . This may relate to the finer Sentinel-1 resolution, as well as to the 1D analysis configuration, having the potential advantage of better representing local hydrologic conditions, such as convective precipitation events. The 3D approach for SMAP has the advantage that it provides smoother transitions, and allows for interpolation and extrapolation of the increments. The joint assimilation ($DA_{\sigma;TB}$) involved both a 3D and 1D filter step, and thus combined the smoothed large scale increments from SMAP with finer-scale increments from Sentinel-1.

Validation of the experiments was based on the correlation coefficient (R [–]) and the unbiased Root Mean Square Difference (ubRMSD [m^3/m^3]), obtained after removing the static long-term mean bias from the simulations and measurements. Metrics are accompanied by 95% confidence intervals (CI), calculated with the assumption of a χ^2 distribution for the ubRMSD, and an asymptotic normal distribution after Fisher Z transformation for R [De Lannoy and Reichle, 2016a]. The CIs account for autocorrelation in the time series by reducing the effective sample size and degrees of freedom [Dawdy and Matalas, 1964; Draper et al., 2012]. Spatial error correlations between nearby sites were accounted for by spatially clustering the results as in Reichle et al. [2017], to avoid that metrics and CIs are dominated by densely sampled areas.

3 Results

Simulated sfmc and rzmc time series were compared with *in situ* measurements at core validation sites and sparse networks (Table 1 and Figure 3). All time steps were included in the evaluation, regardless of whether observations were assimilated.

Sfmc simulations improved increasingly for DA_{σ} , DA_{TB} and $DA_{\sigma;TB}$ (Figure 3). For instance, the R for core sites increased from 0.58 (OL) to 0.63, 0.66 and 0.70, whereas the ubRMSD for core sites decreased from 0.052 (OL) to 0.050, 0.048 and 0.046 m^3/m^3 , respectively (Table 1). Similar results apply for sparse networks. Therefore, this study suggests a better performance when combining SMAP and Sentinel-1 observations in a data assimilation framework. Relative to the SMAP-only assimilation, the joint assimilation increased the improvement by ~30%. However, most improvements were not significant at the 95% level (as indicated by the overlapping CIs). One reason for the lack of significance is in the relatively short data records, which necessarily results in large CIs. Moreover, the CIs were possibly overestimated because of the assumed perfectly correlated errors between sites within the same cluster.

The impact of the Sentinel-1 assimilation may be comparatively small because during most of the experiment period relatively few Sentinel-1 observations were available, particularly outside Europe. While in general larger improvements were observed for DA_{TB} than DA_{σ} , results deteriorated for DA_{TB} (vs. OL) at 3 European sites (REMEDHUS, Twente and HOBE) but yielded improvements for DA_{σ} (Table 1). As previously shown by Lievens et al.

[2016], the joint assimilation alleviates the negative impacts from TB assimilation over those sites, while further enhancing positive impacts over sites where assimilation of both σ^o and TB is beneficial (e.g., Yanco, South Fork, Valencia, Benin). This illustrates the complementary nature of σ^o and TB observations and their relative merits for data assimilation, thereby corroborating the result of Draper et al. [2012].

For rzmc, considerable improvements were obtained for the core site average for all assimilation experiments (Figure 3). However, these improvements are mainly attributed to South Fork, which had a poor performance for OL (Table 1). For other core sites, the impact of DA_{σ^o} was neutral, while DA_{TB} and particularly $DA_{\sigma^o, TB}$ produced moderate improvements over OL. Over sparse networks, no clear impact was observed for any of the assimilation experiments. Overall, the impact was less pronounced for rzmc compared to sfmc.

Finally, it was investigated if the assimilation can also improve the spatial patterns in the estimated sfmc fields for sparse networks in the USA, i.e., SCAN, USCRN and Oklahoma Mesonet (Figure 4). To this end, the spatial correlation between simulations and *in situ* measurements was calculated and averaged over time. Note that combining measurements from different networks may introduce uncertainty in the analysis. Moreover, sparse networks usually contain only a single site per 9-km grid cell, which may or may not be representative of the grid-cell average conditions. Therefore, the results should be interpreted with care.

In a first assessment, all sites were included for all time steps, regardless of whether observations were assimilated. In this case, a minor improvement in spatial R (+0.01) over the OL was observed for DA_{σ^o} , whereas larger R improvements (+0.04 and +0.05) were found for DA_{TB} and $DA_{\sigma^o, TB}$, respectively. However, as only few Sentinel-1 observations were assimilated over the USA (on average 39 per site over the study period), the impact may be concealed. Therefore, in a second assessment, spatial correlations were calculated only for time steps and sites where Sentinel-1 data were assimilated. In this case, improvements in R became comparable for DA_{σ^o} (+0.05) and DA_{TB} (+0.06), and were largest for $DA_{\sigma^o, TB}$ (+0.09). This highlights the potential gain in impact from the assimilation of Sentinel-1 observations with the recent increase in revisit frequency.

4 Conclusions

Sentinel-1 σ^o observations were assimilated either separately from or simultaneously with SMAP TB observations into CLSM, to assess their relative and complementary value for improving soil moisture estimates. The comparison with *in situ* measurements from SMAP core validation sites and sparse networks revealed that assimilation of Sentinel-1 σ^o produces a moderate improvement in surface soil moisture time series, whereas minor impacts were found for the temporal skill of root-zone soil moisture. Larger improvements were obtained with the assimilation of SMAP observations, while the joint assimilation of SMAP and Sentinel-1 observations performed best.

Similar results apply for spatial soil moisture estimation over the USA. The spatial correlation with *in situ* measurements from sparse networks improved increasingly with the assimilation of Sentinel-1, SMAP, and joint observations, respectively. The impact of Sentinel-1 was particularly evidenced when focusing on sites and time steps for which Sentinel-1 observations were assimilated. This result is promising, considering the recent increase in Sentinel-1 data availability going forward.

An increased number of Sentinel-1 observations is expected to benefit the assimilation, not only by more frequent updates of model states, but also by the more accurate processing of observations (e.g., incidence angle normalization and bias correction), and more accurate constraining of the backscatter model. Future study should assess how the increased availability of data will impact hydrologic simulations over the foreseen 12 years of Sentinel-1 operation.

Acknowledgments

The study was performed at the NASA Goddard Space Flight Center in the framework of the HYDRAS+ project (SR/00/302) financed by the Belgian Science Policy (BELSPO). Hans Lievens is a postdoctoral research fellow of the Research Foundation Flanders (FWO). Rolf Reichle is supported by the SMAP Science Team. Computational resources were provided by the NASA High-End Computing Program through the NASA Center for Climate Simulation. We would like to thank the principal investigators and contributors to the *in situ* soil moisture data, including José Martínez-Fernández (REMEDHUS), Rogier van der Velde (Twente), Ernesto Lopez-Baeza (Valencia), Thierry Pellarin (AMMA-CATCH Observatory: Niger and Benin), Todd Caldwell (TxSON), and Simone Bircher (HOBE). We thank the associate editor and reviewers for their valuable contribution to this paper.

References

- Albergel C, et al. Evaluation of remotely sensed and modelled soil moisture products using global ground-based *in situ* observations. *Remote Sensing of Environment*. 2008; 118:215–226.
- Attema E, Ulaby F. Vegetation modeled as a water cloud. *Radio Science*. 1978; 13(2):357–364.
- Bartalis ZK, Scipal K, Wagner W. Azimuthal anisotropy of scatterometer measurements over land. *IEEE Transactions on Geoscience and Remote Sensing*. 2006; 44(8):2083–2092.
- Bell J, et al. U.S. Climate Reference Network soil moisture and temperature observations. *Journal of Hydrometeorology*. 2013; 14:977–988.
- Bircher S, Skou N, Jensen KH, Walker JP, Rasmussen L. A soil moisture and temperature network for SMOS validation in Western Denmark. *Hydrology and Earth System Sciences*. 2012; 16:1445–1463.
- Cappelaere B, et al. The AMMA-CATCH experiment in the cultivated Sahelian area of south-west Niger - Investigating water cycle response to a fluctuating climate and changing environment. *Journal of Hydrology*. 2009; 375:34–51.
- Chan, S., Njoku, EG., Colliander, A. SMAP L1C Radiometer Half-Orbit 36 km EASE-Grid Brightness Temperatures, Version 3. Boulder, Colorado USA: NASA National Snow and Ice Data Center Distributed Active Archive Center; 2016. doi: <http://dx.doi.org/10.5067/E51BSP6V3KP7> [Last accessed 20 March 2017]
- Colliander A, et al. Validation of SMAP surface soil moisture products with core validation sites. *Remote Sensing of Environment*. 2017; 191:215–231.
- Dawdy, D., Matalas, N. *Handbook of Applied Hydrology: A Compendium of Water-Resources Technology*, chap. Statistical and probability analysis of hydrologic data, part III: analysis of variance, covariance and time series. McGraw-Hill; New York: 1964. p. 8.68-8.91.
- De Lannoy GJM, Reichle RH. Global assimilation of multiangle and multipolarization SMOS brightness temperature observations into the GEOS-5 Catchment Land Surface Model for soil moisture estimation. *Journal of Hydrometeorology*. 2016a; 17:669–691.

- De Lannoy GJM, Reichle RH. Assimilation of SMOS brightness temperatures or soil moisture retrievals into a land surface model. *Hydrology and Earth System Sciences*. 2016b; 20:4895–2016.
- De Lannoy GJM, Reichle RH, Pauwels VRN. Global calibration of the GEOS-5 L-band microwave radiative transfer model over nonfrozen land using SMOS observations. *Journal of Hydrometeorology*. 2013; 14(3):765–785.
- De Lannoy GJM, Koster RD, Reichle RH, Mahanama S, Liu Q. An updated treatment of soil texture and associated hydraulic properties in a global land modeling system. *Journal of Advances in Modeling Earth Systems*. 2014a; 6:957–979.
- De Lannoy GJM, Reichle RH, Vrugt JA. Uncertainty quantification of GEOS-5 L-band radiative transfer model parameters using Bayesian inference and SMOS observations. *Remote Sensing of Environment*. 2014b; 148:146–157.
- Diamond H, et al. U.S. Climate Reference Network after one decade of operations: Status and assessment. *Bulletin of the American Meteorological Society*. 2013; 94:485–498.
- Dorigo WA, et al. The International Soil Moisture Network: A data hosting facility for global in situ soil moisture measurements. *Hydrology and Earth System Sciences*. 2011; 15:1675–1698.
- Draper C, Reichle RH, De Lannoy GJM, Liu Q. Assimilation of passive and active microwave soil moisture retrievals. *Geophysical Research Letters*. 2012; 39:L04401.
- Entekhabi, D., et al. Tech. Rep. 400-1567. JPL; 2014. SMAP handbook.
- Entekhabi D, et al. The Soil Moisture Active Passive (SMAP) mission. *Proceedings of the IEEE*. 2010; 98(5):704–716.
- Fung, A. Microwave scattering and emission models and their applications. Artech House; Boston, MA: 1994.
- Geudtner D. Sentinel-1 system overview and performance. *Proceedings of SPIE 8528, Earth Observing Missions and Sensors: Development, Implementation, and Characterization II*. 2012:852802.
- Kerr YH, Waldteufel P, Wigneron JP, Martinuzzi JM, Font J, Berger M. Soil moisture retrieval from space: The Soil Moisture and Ocean Salinity (SMOS) mission. *IEEE Transactions on Geoscience and Remote Sensing*. 2001; 39(8):1729–1735.
- Koster RD, Suarez MJ, Ducharne A, Stieglitz M, Kumar P. A catchment-based approach to modeling land surface processes in a general circulation model: 1. model structure. *Journal of Geophysical Research*. 2000; 105(D20):24809–24822.
- Lebel T, et al. AMMA-CATCH studies in the Sahelian region of West- Africa: An overview. *Journal of Hydrology*. 2009; 375:3–13.
- Lievens H, Martens B, Verhoest NEC, Hahn S, Reichle RH, Miralles DG. Assimilation of global radar backscatter and radiometer brightness temperature observations to improve soil moisture and land evaporation estimates. *Remote Sensing of Environment*. 2016; 189:194–210.
- Liu Q, Reichle RH, Bindlish R, Cosh M, Crow W, De Jeu R, De Lannoy GJM, Huffman GJ, Jackson T. The contributions of precipitation and soil moisture observations to the skill of soil moisture estimates in a land data assimilation system. *Journal of Hydrometeorology*. 2011; 12:750–765.
- Lucchesi, R. Tech. Rep. GMAO Office Note No 4 (Version 1.0). NASA Goddard Space Flight Center; Greenbelt, MD, USA: 2013. File Specification for GEOS-5 FP. <https://ntrs.nasa.gov/search.jsp?R=20150001437>
- Mahanama, S., et al. NASA/TM-2015-104606. Vol. 39. NASA Goddard Space Flight Center; Greenbelt, MD, USA: 2015. Land Boundary Conditions for the Goddard Earth Observing System Model Version 5 (GEOS-5) Climate Modeling System - Recent Updates and Data File Descriptions. <https://ntrs.nasa.gov/search.jsp?R=20160002967>
- McPherson RA, et al. Statewide Monitoring of the Mesoscale Environment: A Technical Update on the Oklahoma Mesonet. *Journal of Atmospheric and Oceanic Technology*. 2007; 24:301–321.
- Pellarin T, Laurent JP, Cappelaere B, Decharme B, Descroix L, Ramier D. Hydrological modelling and associated microwave emission of a semi-arid region in South-western Niger. *Journal of Hydrology*. 2009; 375:262–272.
- Reichle, RH., Liu, Q. NASA/TM-2014-104606. Vol. 35. NASA Goddard Space Flight Center; Greenbelt, MD, USA: 2014. Observation-Corrected Precipitation Estimates in GEOS- 5. <https://ntrs.nasa.gov/search.jsp?R=20150000725>

- Reichle, R.H., De Lannoy, G.J.M., Liu, Q., Ardizzone, J.V., Chen, F., Colliander, A., Conaty, A., Crow, W., Jackson, T., Kimball, J., Koster, R.D., Smith, E.B. Tech. Rep. GMAO Office Note No. 12 (Version 1.0). NASA Goddard Space Flight Center; Greenbelt, MD, USA: 2016. Soil Moisture Active Passive Mission L4_SM Data Product Assessment (Version 2 Validated Release). <https://ntrs.nasa.gov/search.jsp?R=20160008109>
- Reichle R.H., et al. Assessment of the SMAP level-4 surface and root zone soil moisture product using in situ measurements. *Journal of Hydrometeorology*. 2017 submitted.
- Schaefer G.L., Cosh M.H., Jackson T.J. The USDA Natural Resources Conservation Service Soil Climate Analysis Network (SCAN). *Journal of Atmospheric and Oceanic Technology*. 2007; 24:2073–2077.
- Smith A., et al. The Murrumbidgee soil moisture monitoring network data set. *Water Resources Research*. 2012; 48:W07701.
- Su Z., Fernández-Prieto D., Timmermans J., Chen X., Hungershofer K., Roebeling R., Schröder M., Schulz J., Stammes P., Wang P., Wolters E. First results of the earth observation Water Cycle Multi-mission Observation Strategy (WACMOS). *International Journal of Applied Earth Observation and Geoinformation*. 2014; 26:270–285.
- Tuanmu M.-N., Jetz W. A global 1-km consensus land-cover product for biodiversity and ecosystem modeling. *Global Ecology and Biogeography*. 2014; 23(9):1031–1045.
- van der Velde R., Salama M.S., Eweys O.A., Wen J., Wang Q. Soil moisture mapping using combined active or passive microwave observations over the east of the Netherlands. *IEEE Journal of Selected Topics in Applied Earth Observations and Remote Sensing*. 2015; 8:4355–4372.
- Wagner, W., Sabel, D., Doubkova, M., Bartsch, A., Pathe, C. Proc. Earth Observation and Water Cycle Science. Frascati; Italy: 2010. The potential of Sentinel-1 for monitoring soil moisture with a high spatial resolution at global scale.
- Wood E.F., et al. Hyperresolution global land surface modeling: Meeting a grand challenge for monitoring Earth's terrestrial water. *Water Resources Research*. 2011; 47:W05301.
- World Meteorological Organization. Tech. Rep. WMO/TD 1338, GCOS-107. WMO; Geneva, Switzerland: 2006. Systematic Observation Requirements for Satellite-Based Products for Climate.

Key Points

- Sentinel-1 radar and SMAP radiometer observations provide complementary information on soil moisture
- Assimilating Sentinel-1 and SMAP observations improves the spatio-temporal accuracy of soil moisture estimates
- Adding Sentinel-1 data increases the assimilation impact by up to 30%, relative to that of SMAP-only assimilation

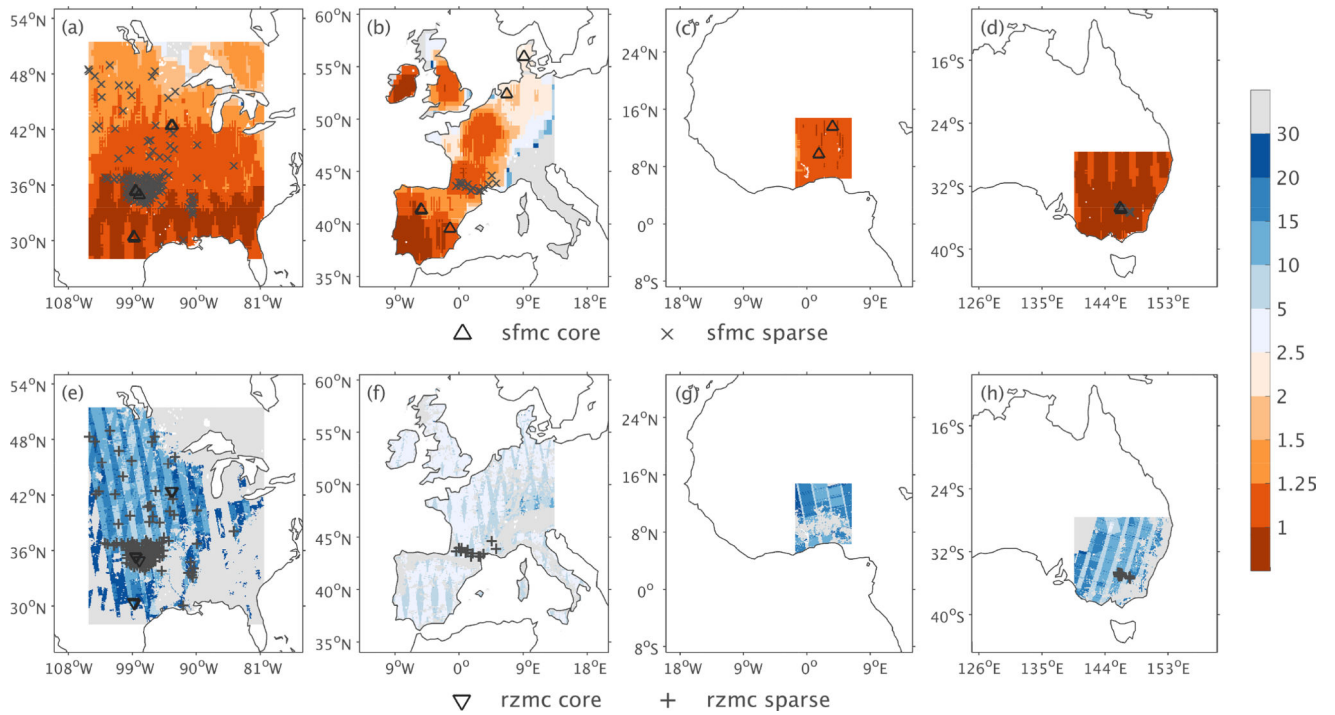


Figure 1. Average time interval [days] between assimilated (a–d) SMAP and (e–h) Sentinel-1 observations over the model domain for May 2015 to December 2016. Symbols show locations of core sites and sparse network sites with (a–d) surface (sfmc) and (e–h) root-zone (rzmc) soil moisture measurements.

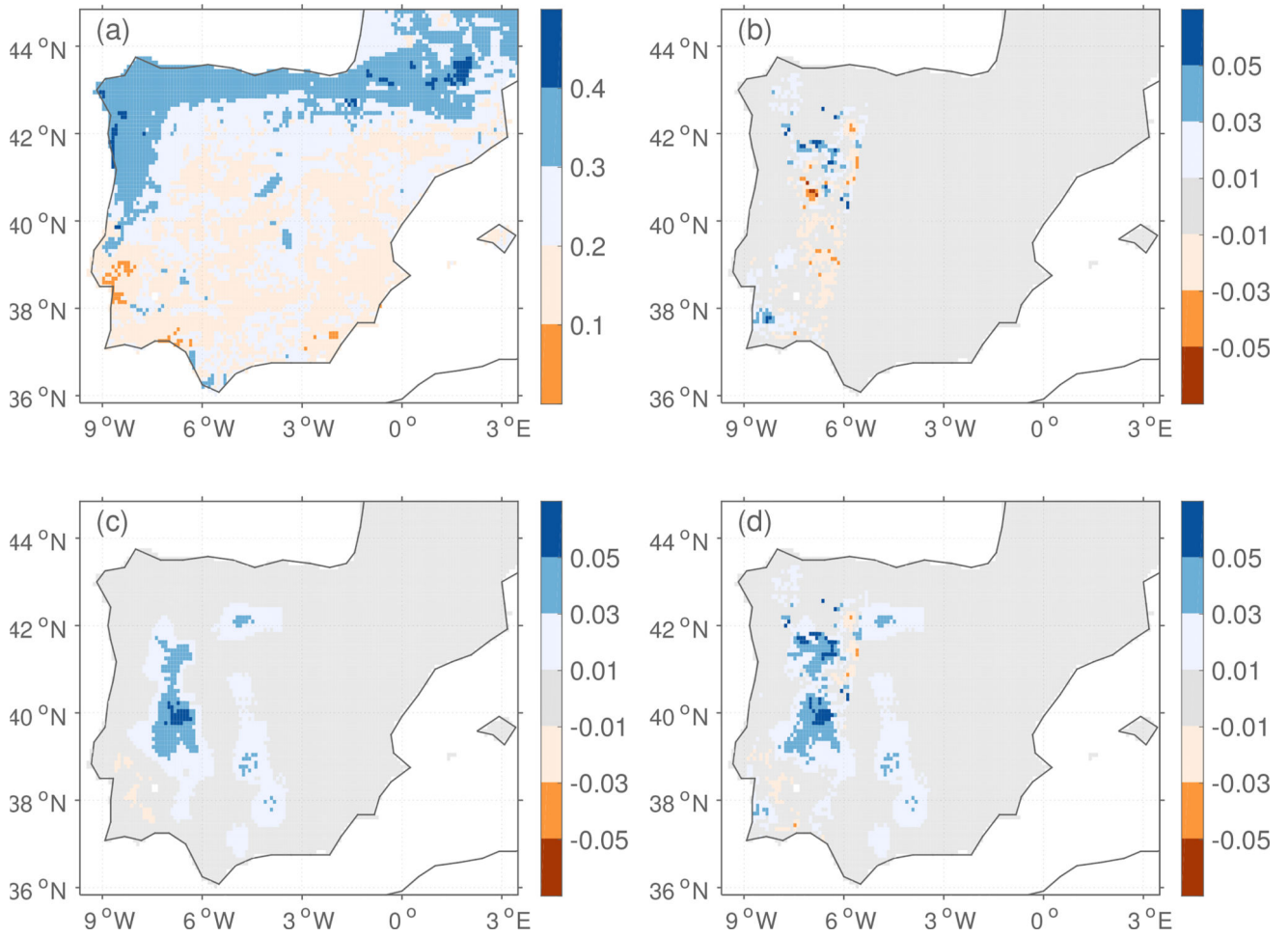


Figure 2.
 The (a) sfmc [m^3/m^3] forecast, and increments [m^3/m^3] for (b) DA_{σ} , (c) DA_{TB} and (d) $DA_{\sigma, TB}$ over Spain, for May, 1, 2015, 6 am.

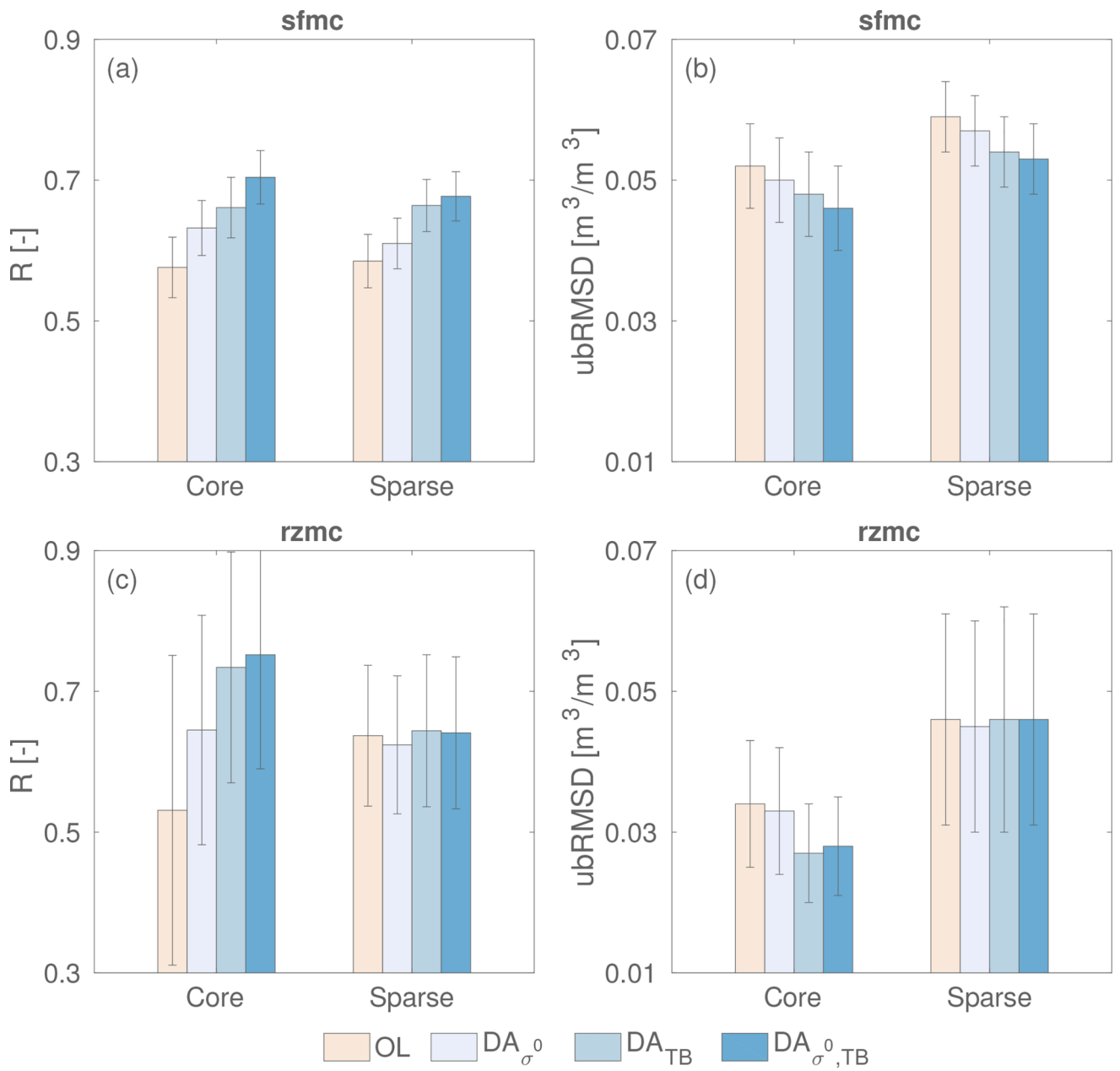


Figure 3. The performance of OL, DA_{σ} , DA_{TB} and $DA_{\sigma,TB}$ for soil moisture simulation: (a,c) R [-] and (b,d) ubRMSD [m^3/m^3] for (a,b) sfmc and (c,d) rzmc. Error bars represent the 95% confidence intervals.

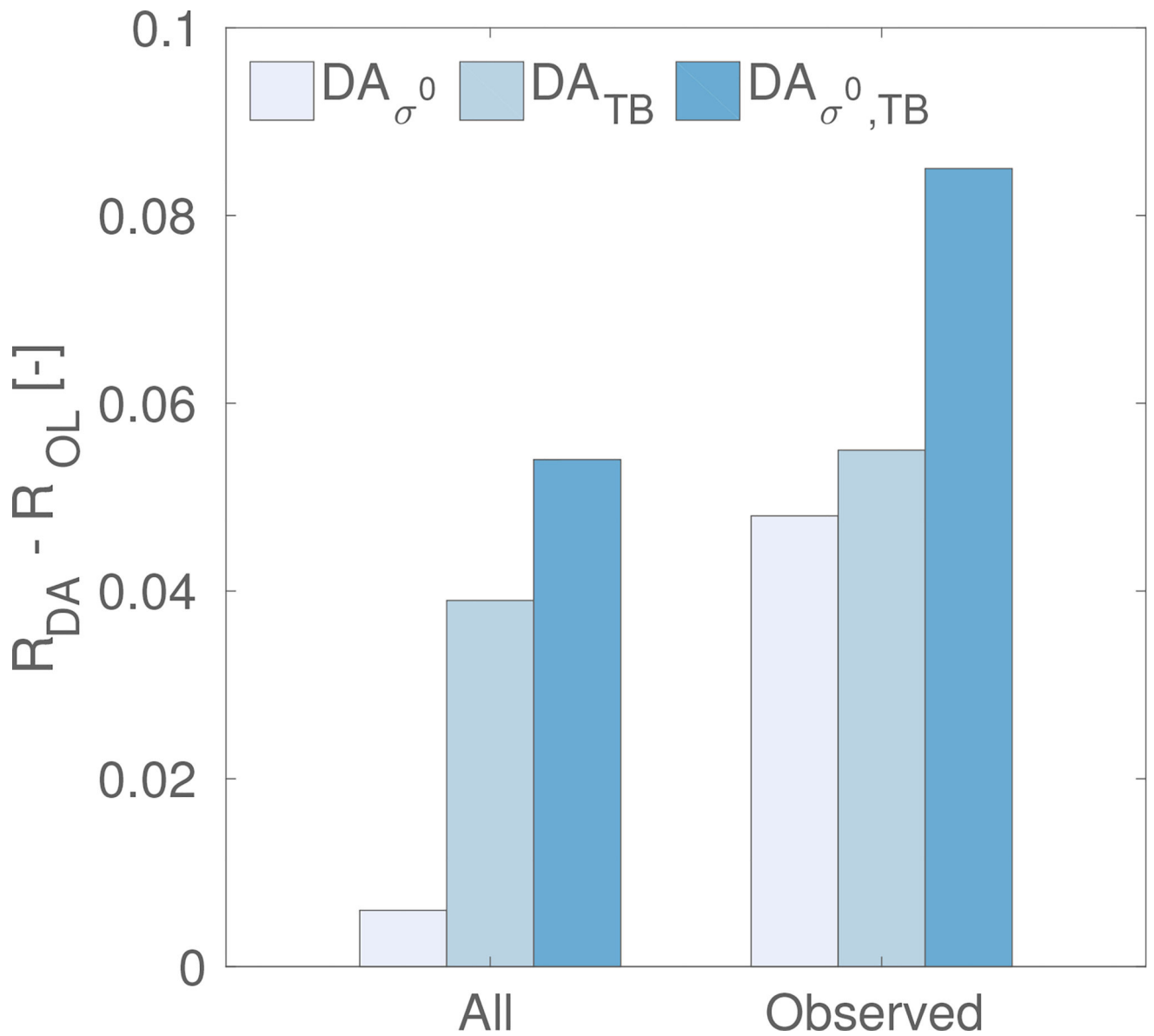


Figure 4. The time-averaged increase in spatial correlation $R [-]$ for the assimilation experiments (relative to the OL) with respect to *in situ* sfmc over sparse networks in the USA (SCAN, USCRN and Oklahoma Mesonet), for all sites and time steps ('All'), and for sites and time steps with Sentinel-1 observations ('Observed').

Table 1

Performance metrics R [-] and $ubRMSD$ [m^3/m^3] of OL , DA_{σ} , DA_{TB} and $DA_{\sigma,TB}$ for surface (sfmc) and root-zone (rzmc) soil moisture. Average metrics for 9-km core sites and sparse networks are followed by the metrics for individual sites/networks. N is the number of grid cells (for core sites) or point measurements (for sparse networks). $N_{in\ situ}$ is the number of 3-hourly *in situ* measurements used for validation. N_{σ} and N_{TB} are the numbers of assimilated Sentinel-1 σ and SMAP TB observations, respectively. SCAN stands for the U.S. Natural Resources Conservation Service Soil Climate Analysis Network, USCRN for the U.S. Climate Reference Network, and SMOSMANIA for the SMOS-Meteorological Automatic Network Integrated Application.

sfmc (0–5 cm)	R [-]													$ubRMSD$ [m^3/m^3]					
	N	$N_{in\ situ}$	N_{σ}	N_{TB}	OL	DA_{σ}	DA_{TB}	$DA_{\sigma,TB}$	CI	OL	DA_{σ}	DA_{TB}	$DA_{\sigma,TB}$	CI	OL	DA_{σ}	DA_{TB}	$DA_{\sigma,TB}$	CI
Core sites	16	2686	75	540	0.58	0.63	0.66	0.70	±0.04	0.052	0.050	0.048	0.046	±0.006					
REMEDHUS	2	2667	127	545	0.59	0.61	0.53	0.60	±0.14	0.032	0.034	0.037	0.035	±0.011					
Yanco	2	3913	42	628	0.84	0.86	0.92	0.93	±0.07	0.079	0.074	0.049	0.049	±0.030					
Twente ¹	1	2611	148	307	0.66	0.81	0.52	0.62	±0.17	0.081	0.076	0.083	0.080	±0.053					
Little Washita	1	2646	78	501	0.70	0.73	0.80	0.79	±0.07	0.041	0.040	0.035	0.035	±0.010					
Fort Cobb	2	4083	78	520	0.64	0.63	0.74	0.74	±0.08	0.043	0.043	0.038	0.037	±0.007					
South Fork	2	3161	45	486	0.10	0.44	0.62	0.67	±0.11	0.069	0.060	0.052	0.050	±0.012					
Valencia	1	1754	94	605	0.39	0.42	0.49	0.51	±0.16	0.026	0.025	0.024	0.024	±0.006					
Niger ²	1	1066	42	595	0.28	0.23	0.47	0.54	±0.17	0.038	0.040	0.049	0.045	±0.006					
Benin ²	1	1821	85	607	0.68	0.71	0.74	0.76	±0.13	0.063	0.062	0.056	0.056	±0.024					
TxSON	2	2177	22	711	0.75	0.77	0.83	0.82	±0.13	0.045	0.044	0.039	0.039	±0.014					
HOBE ³	1	1080	134	248	0.82	0.82	0.73	0.83	±0.13	0.044	0.046	0.051	0.046	±0.026					
Sparse networks	201	3488	49	580	0.59	0.61	0.66	0.68	±0.04	0.059	0.057	0.054	0.053	±0.005					
SCAN ⁴	27	3472	33	544	0.57	0.57	0.64	0.64	±0.04	0.057	0.056	0.056	0.055	±0.006					
USCRN ⁵	25	3288	36	509	0.58	0.60	0.66	0.66	±0.04	0.058	0.057	0.053	0.053	±0.005					
Oklahoma Mesonet ⁶	93	3825	47	585	0.54	0.56	0.67	0.67	±0.09	0.064	0.062	0.058	0.057	±0.013					
OzNet ⁷	42	3405	39	655	0.78	0.79	0.84	0.85	±0.12	0.077	0.073	0.062	0.061	±0.031					
SMOSMANIA ⁸	14	1887	142	512	0.55	0.61	0.62	0.66	±0.14	0.048	0.045	0.045	0.042	±0.014					
rzmc (0–100 cm)																			

sfmc (0–5 cm)	R[–]											ubRMSD [m ³ /m ³]			
	N	N _{in situ}	N _σ	N _{TB}	OL	DA _σ	DA _{TB}	DA _{σ,TB}	CI	OL	DA _σ	DA _{TB}	DA _{σ,TB}	CI	
Core sites	7	2705	52	562	0.53	0.65	0.73	0.75	±0.18	0.034	0.033	0.027	0.028	±0.008	
Little Washita	1	1999	78	501	0.81	0.87	0.84	0.85	±0.17	0.032	0.031	0.027	0.027	±0.012	
Fort Cobb	2	3418	78	520	0.68	0.64	0.68	0.70	±0.26	0.028	0.030	0.031	0.030	±0.009	
South Fork	2	3122	45	486	0.02	0.38	0.57	0.61	±0.32	0.043	0.038	0.030	0.030	±0.009	
TXSON	2	1927	22	711	0.85	0.84	0.90	0.90	±0.37	0.032	0.033	0.023	0.024	±0.023	
Sparse networks	161	3534	51	574	0.64	0.62	0.64	0.64	±0.10	0.046	0.045	0.046	0.046	±0.015	
SCAN	23	3335	35	537	0.65	0.63	0.63	0.62	±0.11	0.041	0.042	0.043	0.042	±0.014	
USCRN	22	3175	37	518	0.64	0.62	0.64	0.63	±0.11	0.046	0.046	0.043	0.043	±0.008	
Oklahoma Mesonet	85	3947	47	587	0.62	0.60	0.64	0.64	±0.36	0.057	0.057	0.056	0.056	±0.075	
OzNet	18	3527	39	667	0.75	0.77	0.81	0.81	±0.66	0.029	0.031	0.054	0.049	±0.176	
SMOSMANIA	13	1799	145	520	0.50	0.55	0.52	0.57	±0.47	0.040	0.038	0.039	0.037	±0.094	

¹ van der Velde et al. [2015].

² Lebel et al. [2009]; Pellarin et al. [2009]; Cappelaere et al. [2009].

³ Bircher et al. [2012].

⁴ Schaefer et al. [2007].

⁵ Diamond et al. [2013]; Bell et al. [2013].

⁶ McPherson et al. [2007].

⁷ Smith et al. [2012].

⁸ Albergel et al. [2008]; Dorigo et al. [2011]